

Geophysical Research Letters

RESEARCH LETTER

10.1029/2019GL083812

Key Points:

- The local climate response to aerosols is strongly modulated by the biophysical attributes of the underlying surface
- Asymmetries between aerosol shortwave and longwave radiative effect reduce the diurnal temperature range, particularly in arid regions
- Long-term enhancement in local climate sensitivity to aerosols is seen in equatorial climate, possibly driven by deforestation

Supporting Information:

- Supporting Information S1

Correspondence to:

T. Chakraborty,
tc.chakraborty@yale.edu

Citation:

Chakraborty, T., & Lee, X. (2019). Land cover regulates the spatial variability of temperature response to the direct radiative effect of aerosols. *Geophysical Research Letters*, 46, 8995–9003. <https://doi.org/10.1029/2019GL083812>

Received 21 MAY 2019

Accepted 13 JUL 2019

Accepted article online 18 JUL 2019

Published online 5 AUG 2019

Corrected 9 AUG 2019

This article was corrected on 9 AUG 2019. See the end of the full text for details.

Land Cover Regulates the Spatial Variability of Temperature Response to the Direct Radiative Effect of Aerosols

T. Chakraborty¹  and X. Lee¹ 

¹School of Forestry and Environmental Studies, Yale University, New Haven, CT, USA

Abstract Aerosol impact on the surface temperature varies between the shortwave and the longwave components of radiation, depends on the time of the day, and is modulated by underlying biophysical processes. We disentangle these complexities by isolating the direct surface shortwave and longwave radiative effects from a global reanalysis data product and calculating their spatially explicit climate sensitivities. Higher sensitivity is found for the longwave component and is driven by a combination of spatial variability of aerosol species and biophysical control of the underlying surface. The opposing shortwave and longwave effects reduce the global mean diurnal temperature range by 0.47 K, with almost half the contribution coming from aerosols of anthropogenic origin. We also find evidence of an increasing trend in the local climate sensitivity in the equatorial zone, possibly caused by deforestation. These surface processes can partially explain why the climate forcing efficacy of aerosols exceeds unity.

Plain Language Summary The radiative effect of aerosols is disproportionately stronger at the Earth's surface compared to the top of the atmosphere and depends on the time of the day and aerosol properties. Moreover, the local surface temperature response to aerosols depends on both incoming energy and the surface energy dissipation via the properties of the underlying surface. To disentangle these complex interactions, we use a theoretical framework to separate surface temperature response to the aerosol shortwave and longwave radiative effects for the world's land surfaces using a reanalysis dataset. We find a stronger local climate sensitivity to the longwave radiative effect than to the shortwave. This is partly due to the incidental collocation of regions of high local climate sensitivity with regions containing coarse mineral dust aerosols. The opposite directions of the surface shortwave and longwave radiative effects reduce the diurnal temperature range, particularly in arid regions. Long-term trends show an intensification of the local climate sensitivity in the tropics due to deforestation, demonstrating the importance of local biophysical processes in aerosol-climate interactions. The addition of this biophysical control may partially explain why the global climate sensitivity to aerosols is stronger than that due to well-mixed greenhouse gases.

1. Introduction

The impact of aerosols is one of the greatest uncertainties in our understanding of the Earth's climate system (Stocker et al., 2013). Aerosols modulate the Earth's radiative budget, either directly through scattering and absorption (Bellouin et al., 2005) or indirectly by influencing the size and longevity of clouds (Li et al., 2011; Twomey, 1991). While several methods can be used to estimate the perturbation to the radiative budget by different forcing agents (Tang et al., 2019), the top of the atmosphere values are traditionally used as a metric for temperature predictions in climate studies. This practice implicitly assumes that the temperature response of the planet is independent of the forcing agent or location of its emission source. While this is defensible for globally homogeneous forcing agents such as well-mixed greenhouse gases, for forcing agents that have significant spatial variability, like land use change, this assumption is insufficient (Bright et al., 2017). Aerosols also fall into this category, due to the significant horizontal and vertical variability of the aerosol radiative effect (RE; Stuber et al., 2005). Because of these spatial heterogeneities, particularly the higher concentration of aerosols over the Northern Hemisphere, the global climate sensitivity to the radiative forcing (RF) of aerosols—the anthropogenic component of the aerosol RE—is higher than the RF associated with well-mixed greenhouse gases (Hansen et al., 2005; Marvel et al., 2015; Rotstayn et al., 2015; Shindell, 2014).

Both the total aerosol RE (Ramanathan et al., 2001) and the relative roles of shortwave and longwave RE depend on altitude (Choobari et al., 2013), aerosol composition, and aerosol size (Hansell et al., 2012; Haywood et al., 1997; Sicard et al., 2014). Overall, the shortwave RE (ΔK_{\downarrow}) dominates the longwave RE (ΔL_{\downarrow} ; Haywood et al., 1997; Highwood et al., 2003; Liao et al., 2004). However, ΔL_{\downarrow} can offset a large portion of ΔK_{\downarrow} in arid and semiarid regions, where coarse-grained mineral dust aerosols are effective emitters of longwave radiation in the atmospheric thermal window (wavelength 4–10 μm ; Choobari et al., 2013). Moreover, ΔL_{\downarrow} exists during both daytime and nighttime unlike ΔK_{\downarrow} . Further complicating the matter is the fact that the same RE can induce very different surface temperature responses because the energy redistribution between the surface and the atmospheric boundary layer varies between time of the day and with the biophysical attributes of the underlying local surface.

Here, we deploy the theory of the intrinsic biophysical mechanism (IBPM; Lee et al., 2011) and an atmospheric reanalysis data product to disentangle these synergistic interactions between the aerosol RE and the local biophysical processes. We aim (1) to quantify spatial variations of the surface shortwave and longwave radiative effects under present climate conditions, (2) to calculate the local surface temperature perturbations caused by these effects, and (3) to discuss the contribution of surface-air exchange processes to the long-term change in the climate efficacy of aerosols.

2. Methods

2.1. The IBPM Theory

The IBPM theory combines the surface energy balance equation with a one-source model of the sensible heat flux to solve for the surface temperature (T_S ; Lee et al., 2011). This solution expresses T_S as a function of atmospheric forcing and energy redistribution between the surface and the lower atmosphere

$$T_S = T_b + \frac{\lambda_0}{1+f} (R_n^* - G) \quad (1)$$

where T_b is the background or blending-height air temperature, λ_0 is the local intrinsic climate sensitivity, f , a dimensionless energy redistribution factor, is a measure of the efficiency of energy dissipation between the surface and the atmospheric boundary layer, G is ground heat flux, and R_n^* is the apparent net radiation given by

$$R_n^* = K_{\downarrow}(1-a) + L_{\downarrow} - \sigma T_b^4 \quad (2)$$

where K_{\downarrow} is the incoming shortwave, L_{\downarrow} is the incoming longwave, a is surface albedo, and σ is the Stefan-Boltzmann constant. The local intrinsic climate sensitivity is essentially the longwave feedback derived by differentiating the Stefan-Boltzmann law and is given by

$$\lambda_0 = \frac{1}{4\epsilon\sigma T_b^3} \quad (3)$$

Changes to T_S are produced via perturbations to the energy redistribution and to the forcing variables T_b and R_n^* .

The aerosol direct effect changes T_S by perturbing T_b , K_{\downarrow} and L_{\downarrow} at the surface, and f . Differentiating equation (1), we obtain

$$\Delta T_S = \Delta T_b + \Delta T - \frac{\lambda_0}{(1+f)^2} (R_n^* - G) \Delta f \quad (4)$$

where Δ indicates the perturbation signal. Perturbation to the energy redistribution factor Δf can arise from changes in Bowen ratio as a response to more diffuse radiation under polluted skies or from changes in land use that alters the surface roughness. ΔT can be separated into the contributions from the aerosol surface ΔK_{\downarrow} and ΔL_{\downarrow} as

$$\Delta T = \frac{\lambda_0}{1+f} [(1-a)\Delta K_{\downarrow} + \Delta L_{\downarrow}] \quad (5)$$

where the effective local climate sensitivity is given by

$$\lambda^* = \frac{\lambda_0}{1+f} \quad (6)$$

Note that the local surface temperature perturbation (ΔT), when added to the background temperature change (ΔT_b), gives the total surface temperature change (ΔT_s). In this study, we estimate this ΔT from (1) ΔK_{\downarrow} and ΔL_{\downarrow} derived from the radiation diagnostics with and without aerosols and (2) f from the lowest level modeled temperature and the reanalyzed surface energy balance variables (Bright et al., 2017; Lee et al., 2011) from the Modern-Era Retrospective analysis for Research and Applications global reanalysis product (version 2; MERRA-2; Gelaro et al., 2017).

2.2. Reanalysis Data Product

The MERRA-2 data are gridded at a spatial resolution of 0.625° by 0.5° for every hour. In addition to standard meteorological variables and radiative fluxes under realistic conditions, MERRA-2 calculates the diagnostic radiative flux by assuming no aerosols in the atmosphere. The direct aerosol effect is then determined from these radiation fields. In the case of the shortwave RE, ΔK_{\downarrow} is the difference in K_{\downarrow} between all-sky and polluted conditions versus all-sky and clean conditions (Figures 1e and 1f). In the case of the longwave RE, ΔL_{\downarrow} is the difference in L_{\downarrow} absorbed by the surface under all-sky and polluted conditions versus clear-sky and clean conditions (Figures 1g and S2a in the supporting information). This hybrid approach (all-sky for K_{\downarrow} and clear sky for L_{\downarrow}) is used since MERRA-2 does not provide all-sky incoming L_{\downarrow} without aerosols.

Additionally, the MERRA-2 dataset is used to compute f by inverting equation (1)

$$f = \frac{\lambda_0}{T_s - T_b} (R_n^* - G) - 1 \quad (7)$$

In this diagnostic calculation, T_b is the air temperature at the lowest model level (985 hPa), and all other variables are obtained from the suite of surface micrometeorological variables produced by the reanalysis. The median f values for each year are calculated separately for daytime and nighttime for each grid. The annual mean values are averages of the daytime and nighttime values weighted by the daytime and nighttime hours for each grid. For all variables, data from the most recent decade (2008 to 2017) are used to produce mean spatial patterns, and data from the full assimilation period (1980 to 2017) are used to examine temporal trends.

The global spatial pattern of daytime f (Figure S1a) is broadly similar to the f map given in Bright et al. (2017) for the period from 2001 to 2011. In Bright et al. (2017), the f value was computed from a satellite- and surface-based observational dataset using the same diagnostic equation (equation (7)). Our global mean f of 4.21 (supporting information Table S1) compares favorably to the global mean of around 3.67 reported in Bright et al. (2017). As expected, f is lower for smooth surfaces and higher for rough surfaces. Due to the predominance of forested (rougher) areas in tropical latitudes, the f value is much higher near the equator than at other latitudes. A strong diurnal asymmetry exists in f , with much lower values at night resulting from higher static stability and less turbulent mixing than during the day.

2.3. Isolating the Impact of Aerosols by Climate Zone

Given that we focus on the Earth's land surfaces in this study, all global mean values, unless specified otherwise, refer to the spatial means over the MERRA-2 grids that are predominantly (>90%) land. To investigate the role of surface characteristics on aerosol-surface interactions, we divide the world's land surfaces into the Koppen-Geiger climate classes, namely, equatorial, arid, warm temperate (henceforth, temperate), snow, and polar (Rubel & Kotteck, 2010), representing five different regimes of surface characteristics and atmospheric forcing (Figure S4a). Regional mean values are computed from spatial averaging within these regions of interest.

2.4. Contribution of Anthropogenic Aerosols to Radiative Effect

A second group of regions of interest are used to estimate the anthropogenic aerosol contribution to the ΔT . They are the following: United States, South America, OECD Europe, Southern Africa, Russia, East Asia, South Asia, and South East Asia. These regions are chosen based on a previous study, in which researchers ran the Goddard Chemistry, Aerosol, Radiation, and Transport (GOCART) model using emission

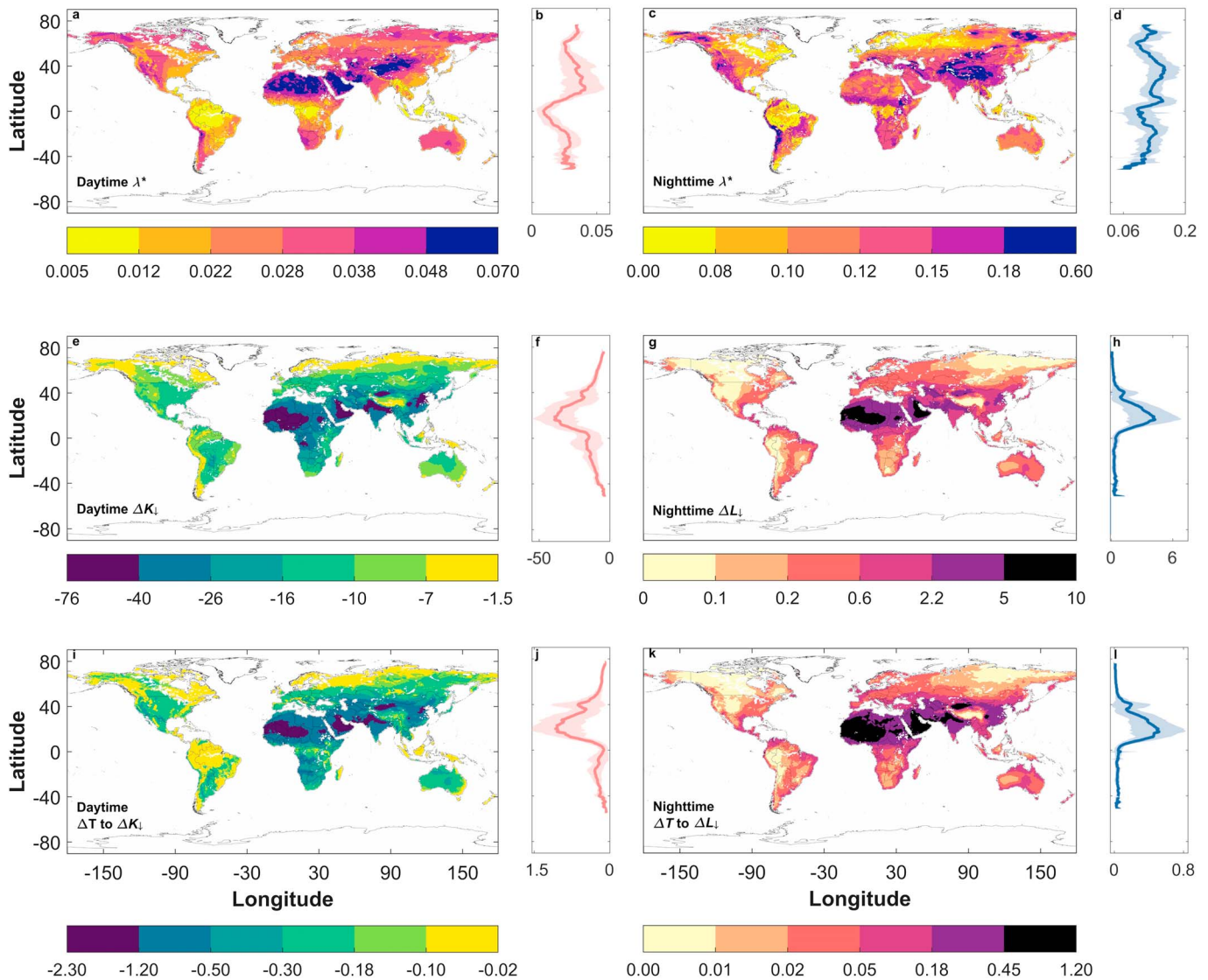


Figure 1. Global spatial patterns of daytime (a) and nighttime (c) apparent surface climate sensitivity λ^* (in $\text{K W}^{-1} \text{m}^2$), daytime shortwave radiative effect RE (e, ΔK_I ; in W m^{-2}), nighttime longwave RE (g, ΔL_I ; in W m^{-2}), daytime temperature perturbation ΔT due to shortwave RE (in K; i), and nighttime ΔT due to longwave RE (in K; k) for 2008–2017. Nonlinear color maps are used to better visualize the spatial variations throughout the world. The corresponding zonal characteristics are also given in panels b (daytime λ^*), d (nighttime λ^*), f (daytime shortwave RE), h (nighttime RE), j (daytime ΔT), and l (nighttime ΔT). The solid lines represent the zonal means, while the shaded regions show standard deviations at each degree of latitude

inventories for anthropogenic and natural aerosol sources and quantified the anthropogenic contribution to the aerosol optical depth (AOD) for each aerosol species (Streets et al., 2009).

At the surface, changes in ΔK_I are proportional to changes in AOD. Thus, for each region of interest, the fractional contribution of anthropogenic aerosols to ΔK_I is equal to the fractional contribution of these aerosols to the total AOD. The anthropogenic AOD fractions for these regions are taken from Streets et al. (2009). The AOD calculated by MERRA-2 for the five main aerosol species (dust, sea salt, sulphate, organic carbon, and black carbon) is in excellent agreement with the results of Streets et al. (2009; Figure S4b), indicating broad consistence between MERRA-2 and GOCART. The anthropogenic contribution to ΔT for aerosol RE (shortwave) is obtained from equation (5) using anthropogenic ΔK_I .

To obtain the anthropogenic contribution to ΔL_I , we first convert the total assimilated AOD at 550 nm from MERRA-2 to the AOD at 10,000 nm (roughly the middle of the longwave wavelength band) for each aerosol species using the Angstrom power law (Ångström, 1929);

$$\text{AOD}_{10000} = \text{AOD}_{550} \left[\frac{10000}{550} \right]^{-\mathring{A}} \quad (8)$$

where \mathring{A} is the Angstrom exponent for the wavelength-dependence of AOD for that species. Of the five aerosol species, we assume that all sulphate, organic carbon, and black carbon aerosols originate from anthropogenic sources and that all dust and sea-salt aerosols originate from natural sources. We then obtain the total fractional contribution of anthropogenic aerosols to the total AOD at 10,000 nm. The anthropogenic contribution to ΔL_{\downarrow} is the product of ΔL_{\downarrow} and this AOD fraction. Strictly, \mathring{A} is based on the AOD at two wavelengths and is valid within the range bounded by the two wavelength values used. For instance, MERRA-2's \mathring{A} is based on the AOD at 470 and 870 nm. Beyond this range, linear extrapolation using \mathring{A} can lead to uncertainties (Kedia & Ramachandran, 2009). Moreover, some of the sulphate, organic carbon, and black carbon aerosols are produced by natural sources. For these reasons, we consider our estimates of the anthropogenic contribution to ΔL_{\downarrow} to be upper bounds of the actual values. The overall results are not affected by these simplifications because the anthropogenic ΔL_{\downarrow} fraction is almost negligible, varying from 2% to 6% in the regions of interest, and consistent with previous estimates (Stier et al., 2007).

3. Results

3.1. Local Temperature Response to Aerosol Direct Radiative Effect

The surface ΔK_{\downarrow} is most negative over eastern China, North India, and western Africa owing to high pollution and dust emissions (Figure 1e). Due to the strong interaction between dust aerosols and L_{\downarrow} , the surface ΔL_{\downarrow} shows large positive values over arid regions, namely, the Sahara Desert, the Arabian Peninsula, northwestern China, and western India (Figures 1g and S2a). In heavily polluted parts of eastern China and North India, the daytime ΔL_{\downarrow} is around 3.5 W m^{-2} or about 30% of the highest value found for Sahara Desert. The global mean daytime ΔK_{\downarrow} over land is -16.40 W m^{-2} , or 16 times the magnitude of the daytime (1.01 W m^{-2} ; Figure S2a) and nighttime ΔL_{\downarrow} (0.99 W m^{-2} ; Figure 1g). The annual mean ΔK_{\downarrow} over the whole planet (land + oceans) is -4.31 W m^{-2} .

The surface temperature response to aerosols is controlled by both the local RE and the local climate sensitivity. The daytime local climate sensitivity λ^* is highest over the arid and polar climate zones due to the lack of vegetation and is lowest in the equatorial zone because high surface roughness promotes energy redistribution between the surface and the lower atmosphere (Figure 1a). We have already noted the high RE over the arid zone. λ^* is also high, implying that this zone is most sensitive to aerosol loading. The presence of coarse mode aerosols that strongly affect L_{\downarrow} over these regions, combined with the overall higher surface reflectivity for K_{\downarrow} , leads to a stronger daytime sensitivity to ΔL_{\downarrow} ($0.039 \text{ K W}^{-1} \text{ m}^2$) than to ΔK_{\downarrow} ($0.024 \text{ K W}^{-1} \text{ m}^2$) when averaged over the Earth's land surfaces. The nighttime λ^* is more than twice as much as the daytime value, indicating less turbulent mixing during this period and resulting in a much stronger temperature response to the same RE than during the day. There is less variability in λ^* among the different climate zones at night than during the day (Figure 1c). The mean surface climate sensitivity to surface aerosol RE for the Earth's land surface is $0.016 \text{ K W}^{-1} \text{ m}^2$, estimated by dividing the global mean ΔT of -0.13 K with the global mean surface RE (including both shortwave and longwave) of -7.94 W m^{-2} (supporting information Table S1). This local surface climate sensitivity is more than an order of magnitude smaller than the global climate sensitivity derived from radiative balance perturbations at the top of the atmosphere (Rotstayn et al., 2015).

The IBPM calculation reveals highly variable but spatially coherent patterns of ΔT across the world (Figures 2i, 2k, and S2c). These spatial patterns are largely controlled by the spatial variabilities of ΔK_{\downarrow} and ΔL_{\downarrow} and are also influenced by local biophysical processes. The global mean daytime ΔT over land is -0.39 K due to ΔK_{\downarrow} and 0.04 K due to ΔL_{\downarrow} , while the nighttime ΔT is 0.13 K due to ΔL_{\downarrow} . Regionally, the strongest response is seen in the arid zone, with the daytime ΔT reaching around -2.3 K and nighttime ΔT reaching 1.2 K . The zonal mean ΔT peaks at around 20°N for both shortwave (-1.1 K) and longwave (0.2 K in the daytime and 0.5 K during nighttime) due to the high climate sensitivity (in the daytime; Figure 1b) and the high RE (both daytime and nighttime, Figures 1f, 1h, and S2b). Averaged over the 24-hr cycle, the aerosol direct RE reduces the global surface temperature by 0.13 K during 2008 to 2017 (supporting information Table S1). In some regions (like Australia), the nighttime warming due to ΔL_{\downarrow} is large enough to almost offset the daytime cooling due to ΔK_{\downarrow} (Figure 1).

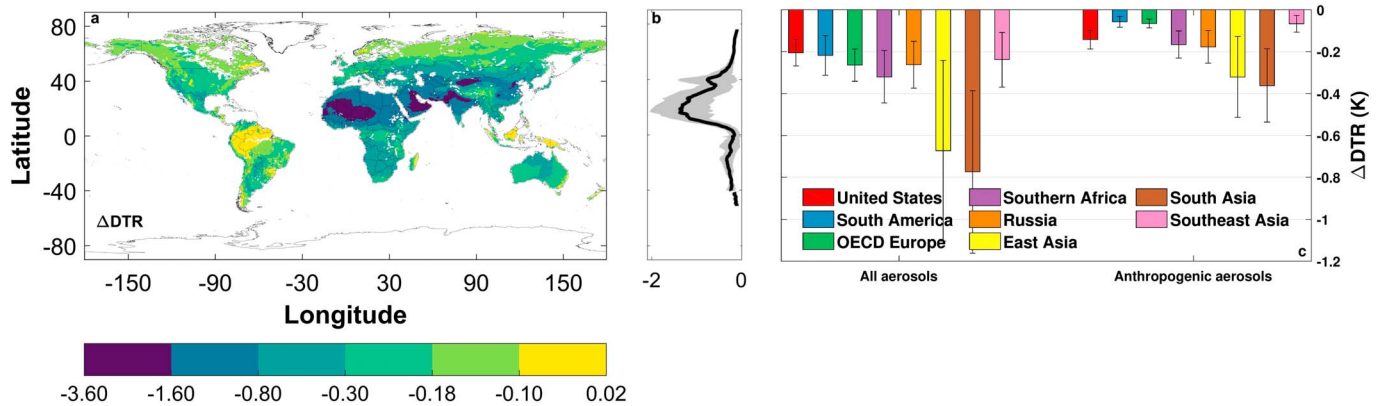


Figure 2. **a**, Global spatial pattern of changes in the diurnal temperature range (DTR; in K) for 2008–2017, **b**, zonal mean change in DTR, and **c**, mean DTR change for each region of interest due to all aerosols and only anthropogenic aerosols. Shaded regions in panel **b** and error bars in panel **c** represent ± 1 standard deviation.

3.2. Impact on the Diurnal Temperature Range and Anthropogenic Contributions

The daytime cooling and nighttime warming will reduce the diurnal temperature range (DTR) (Huang et al., 2006; Sarangi et al., 2018). Although this aerosol DTR effect is known conceptually for some time, we lack a detailed assessment of its geographic variation and a quantitative attribution of anthropogenic and natural contributions. Here, we find that unsurprisingly, the highest reduction in DTR (around 3 K) occurs over arid regions with high aerosol loading (Figure 2). In the Amazon basin, because the effective climate sensitivity is extremely low (daytime $\lambda^* = 0.0075 \text{ K W}^{-1} \text{ m}^2$), aerosols have little impact on DTR (around -0.09 K) even though ΔK_{\downarrow} and ΔL_{\downarrow} are moderately strong, at -10.55 and 0.28 W m^{-2} , respectively. For comparison, similar REs ($\Delta K_{\downarrow} = -9.56 \text{ W m}^{-2}$; $\Delta L_{\downarrow} = 0.44 \text{ W m}^{-2}$) cause a larger reduction in DTR (-0.27 K) in Australia, where smooth landscapes, which are not efficient at dissipating heat from the surface to the atmospheric boundary layer, enhance the climate sensitivity (daytime $\lambda^* = 0.0299 \text{ K W}^{-1} \text{ m}^2$).

Anthropogenic aerosols account for around 10% of the total global aerosol load (Hinds, 1999), but because they have higher scattering efficiencies than natural aerosols, they contribute to almost half the AOD, thus disproportionately modulating the surface temperature response. Averaged over the eight major regions of the world considered here, anthropogenic aerosols reduce the surface K_{\downarrow} by 8.2 W m^{-2} and increase the surface L_{\downarrow} by 0.022 W m^{-2} (Figure S5) through their direct effect. The anthropogenic contribution to the overall DTR reduction is highest for the United States at 68% and lowest for South America at 26%. Aggregating all the eight regions of interest, anthropogenic aerosols lead to about 50% of the total DTR reduction (Figure 2c).

3.3. Interannual Trends

Globally, the ΔT becomes more negative at a rate of -0.014 K per decade in the daytime for shortwave and more positive at a rate of 0.002 K (daytime) and 0.006 K (night) per decade for longwave, from 1980 to 2017 (Figure 3). The combined effect is a decrease of the global DTR by -0.018 K per decade (Figure S11). The primary driver of these global temperature trends is the strengthening of the aerosol RE over time. The mean ΔK_{\downarrow} and daytime (nighttime) ΔL_{\downarrow} are -16.4 and 1.01 (0.99) W m^{-2} in 2008–2017, respectively, compared to -14.6 and 0.88 (0.88) W m^{-2} in 1980–1989. Note that the differences in the first and last 10-year means are muted due to aerosol loading caused by the volcanic eruption of El Chichón in 1982. Of the five climate zones (Figures 3 and S6 to S9), the temperate zone experiences the largest percentage change between the first and last 10 years for ΔK_{\downarrow} (22%) and ΔL_{\downarrow} (44% during day, 50% at night).

Regionally, the most notable feature is a steady increase of daytime λ^* , or a progressive reduction of efficiency of energy redistribution over time, in the equatorial zone (Figure 3a). We attribute this trend to the wide-scale deforestation in the tropics (Achard et al., 2002; Hansen et al., 2013). Although the MERRA-2 modeling system does not explicitly prescribe land use change over time, it uses the observed surface climate variables to constrain the surface energy balance calculation. Tropical deforestation appears to have changed the surface climate so as to result in the diagnosis by the reanalysis of a loss in the efficiency of energy redistribution between the surface and the atmospheric boundary layer. This loss of forest cover serves to amplify the

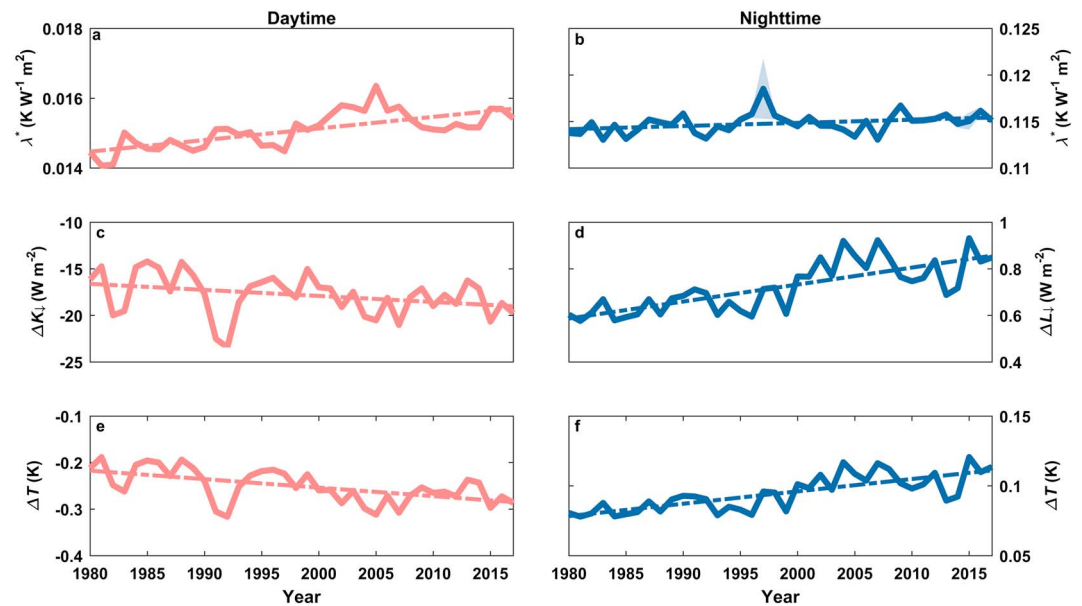


Figure 3. Long-term trends in **a**, daytime apparent surface climate sensitivity λ^* , **b**, nighttime λ^* , **c**, daytime surface shortwave RE (ΔK_{\downarrow}), **d**, nighttime surface longwave RE (ΔL_{\downarrow}), **e**, daytime temperature perturbation, and **f**, nighttime temperature perturbation for the equatorial climate zone. The dashed lines show the linear trends of the temporal variation. All long-term trends are statistically significant (p value < 0.01).

aerosol effect. Sensitivity calculations using equation (5) show that of the increase of the daytime cooling signal of 0.067 K between 1980 and 2017, about one third is attributed to the reduction in λ^* (and the other two third to changes in ΔK_{\downarrow}). Nonradiative surface pathways, such as the energy redistribution efficiency, are shown to dominate the surface temperature change associated with ongoing land cover change and land management activities (Alkama & Cescatti, 2016; Bright et al., 2017; Naudts et al., 2016). Our result suggests that these surface processes can also modify local temperature changes resulting from atmospheric radiative forcing.

4. Discussion

Previous studies have shown that the climate sensitivity associated with aerosol RF is greater than that to CO_2 RF (Marvel et al., 2015; Rotstayn et al., 2015; Shindell, 2014). Estimates based on single-forcing model experiments reveal that the former is about $0.55 \text{ K W}^{-1} \text{ m}^2$ and the latter is $0.40 \text{ K W}^{-1} \text{ m}^2$ under transient climate conditions (Marvel et al., 2015), giving a sensitivity difference of $0.15 \text{ K W}^{-1} \text{ m}^2$ and a climate forcing efficacy of 1.4 for aerosols. Geographic variations in aerosols are suggested to play a role in producing this large efficacy (Boucher et al., 2013), but the nature of this role is not well understood. Our study provides a mechanistic explanation for why the efficacy of aerosol RF should exceed unity. In the IBPM framework, the surface temperature perturbation (ΔT) is a signal superimposed on changes in the background atmospheric temperature (ΔT_b , equation (4)). The total surface temperature change is the sum of the two. CO_2 , a spatially homogeneous forcing agent, alters the energy balance of the climate system as a whole, leading to changes in the background atmospheric temperature, but it does not change the surface incoming solar radiation in predictable patterns either spatially or temporally (Wild et al., 2015). In other words, if CO_2 is the only radiative forcing agent, we can omit the surface temperature perturbation due to the surface K_{\downarrow} . On the other hand, aerosols alter both the whole Earth system energy balance and radiation incident on the surface. We postulate that it is this strong surface RE that results in the large overall aerosol climate efficacy. In our analysis, we assume that the background temperature change (ΔT_b) can be predicted by the energy imbalance measured at the top of the atmosphere using a standard climate sensitivity value and the additional temperature change (ΔT) is the result of the intrinsic surface biophysical mechanism. It is the latter that explains why the aerosol climate forcing efficacy is greater than unity.

Our calculations suggest that the aerosol direct effect alone can explain the large climate efficacy of aerosols, without consideration of the aerosol indirect effect. The mean surface climate sensitivity to aerosol RE

reported above ($0.016 \text{ K W}^{-1} \text{ m}^2$) is based on the surface RE. If we divide the global mean land surface ΔT (-0.13 K) by the combined shortwave and longwave RE at the top of the atmosphere in MERRA-2 (-0.89 W m^{-2} ; supporting information Table S1), we obtain a sensitivity of around $0.15 \text{ K W}^{-1} \text{ m}^2$ attributed to the intrinsic biophysical mechanism, which is nearly the same as the difference ($0.15 \text{ K W}^{-1} \text{ m}^2$) between the aerosol and the CO_2 climate sensitivity (Marvel et al., 2015). Note that accurate calculations of climate sensitivities necessitate examining temperature changes over both land and ocean surfaces. While we only focus on the world's land surfaces, we demonstrate that the local climate response driven by land-atmosphere interactions below the blending height can conceptually explain the higher global climate sensitivity to aerosols.

From this aggregated assessment, we have excluded the temperature perturbation that may arise from changes in the energy redistribution factor f (the last term on the right-hand side of equation (4)). We have already noted that land use change at tropical latitudes has amplified the aerosol effect through reducing f and increasing the local apparent climate sensitivity, although globally, the temporal trend in local apparent climate sensitivity is negligible (Figure S10). A second process that can alter f is changes in the diffuse radiation. Aerosol scattering increases the fraction of diffuse radiation received by the surface, allowing sunlight to penetrate vegetation canopies and increase the gross primary productivity of the land biosphere (Mercado et al., 2009; Rap et al., 2018) and the fraction of heat transferred through evapotranspiration, thus decreasing the Bowen ratio (Liu et al., 2014). We are unable to isolate this biological response to diffuse radiation from the MERRA-2 dataset since MERRA-2 only provides diffuse radiation under polluted conditions. According to a global modeling study, the presence of aerosols can reduce the land Bowen ratio by 15% to 30% between 20°N and 20°S (Liu et al., 2014). In principle, a reduction in Bowen ratio will generate a negative surface temperature perturbation in the daytime due to changes in f (Lee et al., 2011) in addition to the negative perturbation due to the shortwave RE. An accurate estimate of this Bowen ratio induced signal requires that a land surface model be coupled with an atmospheric radiation transfer model to simultaneously calculate the surface incoming radiation (including changes in the diffuse fraction) and the response of the surface sensible and latent heat fluxes.

5. Conclusions

In this study, we disentangle the local temperature response to the direct surface shortwave and longwave radiative effects of aerosols for the world's land surfaces. We find that the global mean climate sensitivity to the surface longwave effect during the daytime ($0.039 \text{ K W}^{-1} \text{ m}^2$) is 60% stronger than to the daytime surface shortwave effect ($0.024 \text{ K W}^{-1} \text{ m}^2$) and 5 times as strong at night ($0.127 \text{ K W}^{-1} \text{ m}^2$). The former is a consequence of higher emissions of coarse aerosols in regions where the surface energy redistribution is less efficient, and the latter is related to low turbulent mixing in stable nighttime conditions. The opposing longwave and shortwave effects reduce the DTR, particularly in arid regions, with almost half the global mean reduction attributable to anthropogenic aerosols. Finally, we analyze long-term trends in the surface temperature response to aerosol direct radiative effect and find an increase in the local climate sensitivity in the equatorial zone, possible driven by deforestation activities. Our results demonstrate the importance of biophysical processes in modulating the spatial heterogeneity of aerosol-climate interactions. The inclusion of this local climate response to aerosols may explain their higher climate forcing efficacy.

Acknowledgments

We acknowledge Yale Center for Earth Observation (YCEO) for providing computational resources. The reanalysis dataset used in this study can be found on NASA's website (<https://gmao.gsfc.nasa.gov/reanalysis/MERRA-2/>).

References

- Achard, F., Eva, H. D., Stibig, H. J., Mayaux, P., Gallego, J., Richards, T., & Malingreau, J. P. (2002). Determination of deforestation rates of the world's humid tropical forests. *Science*, *297*(5833), 999–1002. <https://doi.org/10.1126/science.1070656>
- Alkama, R., & Cescatti, A. (2016). Biophysical climate impacts of recent changes in global forest cover. *Science*, *351*(6273), 600–604. <https://doi.org/10.1126/science.aac8083>
- Ångström, A. (1929). On the atmospheric transmission of sun radiation and on dust in the air. *Geografiska Annaler*, *11*(2), 156–166.
- Bellouin, N., Boucher, O., Haywood, J., & Reddy, M. S. (2005). Global estimate of aerosol direct radiative forcing from satellite measurements. *Nature*, *438*(7071), 1138–1141. <https://doi.org/10.1038/nature04348>
- Boucher, O., Randall, D., Artaxo, P., Bretherton, C., Feingold, G., Forster, P., et al. (2013). Clouds and aerosols. In *Climate Change 2013 - The Physical Science Basis*, (pp. 571–658). Cambridge: Cambridge Univ. Press.
- Bright, R. M., Davin, E., O'Halloran, T., Pongratz, J., Zhao, K., & Cescatti, A. (2017). Local temperature response to land cover and management change driven by non-radiative processes. *Nature Climate Change*, *7*(4), 296–302. <https://doi.org/10.1038/nclimate3250>
- Choobari, O. A., Zawar-Reza, P., & Sturman, A. (2013). Simulation of the spatial distribution of mineral dust and its direct radiative forcing over Australia. *Tellus Series B: Chemical and Physical Meteorology*, *65*(1), 19856. <https://doi.org/10.3402/tellusb.v65i0.19856>
- Gelaro, R., McCarty, W., Suárez, M. J., Todling, R., Molod, A., Takacs, L., et al. (2017). The Modern-Era Retrospective Analysis for Research and Applications, Version 2 (MERRA-2). *Journal of Climate*, *30*(14), 5419–5454. <https://doi.org/10.1175/JCLI-D-16-0758.1>

- Hansell, R. A., Tsay, S. C., Hsu, N. C., Ji, Q., Bell, S. W., Holben, B. N., et al. (2012). An assessment of the surface longwave direct radiative effect of airborne dust in Zhangye, China, during the Asian Monsoon Years field experiment (2008). *Journal of Geophysical Research*, *117*, D00K39. <https://doi.org/10.1029/2011JD017370>
- Hansen, J. E., Sato, M. K. I., Ruedy, R., Nazarenko, L., Lacis, A., Schmidt, G. A., et al. (2005). Efficacy of climate forcings. *Journal of Geophysical Research*, *110*, D18104. <https://doi.org/10.1029/2005JD005776>
- Hansen, M. C., Potapov, P. V., Moore, R., Hancher, M., Turubanova, S. A. A., Tyukavina, A., et al. (2013). High-resolution global maps of 21st-century forest cover change. *Science*, *342*(6160), 850–853. <https://doi.org/10.1126/science.1244693>
- Haywood, J. M., Roberts, D. L., Slingo, A., Edwards, J. M., & Shine, K. P. (1997). General Circulation Model calculations of the direct radiative forcing by anthropogenic sulfate and fossil-fuel soot aerosol. *Journal of Climate*, *10*(7), 1562–1577. [https://doi.org/10.1175/1520-0442\(1997\)010<1562:GCMCOT>2.0.CO;2](https://doi.org/10.1175/1520-0442(1997)010<1562:GCMCOT>2.0.CO;2)
- Highwood, E. J., Haywood, J. M., Silverstone, M. D., Newman, S. M., & Taylor, J. P. (2003). Radiative properties and direct effect of Saharan dust measured by the C-130 aircraft during Saharan Dust Experiment (SHADE): 2. Terrestrial spectrum. *Journal of Geophysical Research*, *108*(D18), 8578. <https://doi.org/10.1029/2002JD002552>
- Hinds, C. W. (1999). *Aerosol technology: Properties, behavior, and measurement of airborne particles*, (Vol. 2). Hoboken, NJ: A Wiley-Interscience Publication.
- Huang, Y., Dickinson, R. E., & Chameides, W. L. (2006). Impact of aerosol indirect effect on surface temperature over East Asia. *Proceedings of the National Academy of Sciences*, *103*(12), 4371–4376. <https://doi.org/10.1073/pnas.0504428103>
- Kedia, S., & Ramachandran, S. (2009). Variability in aerosol optical and physical characteristics over the Bay of Bengal and the Arabian Sea deduced from Ångström exponents. *Journal of Geophysical Research*, *114*, D14207. <https://doi.org/10.1029/2009JD011950>
- Lee, X., Goulden, M. L., Hollinger, D. Y., Barr, A., Black, T. A., Bohrer, G., et al. (2011). Observed increase in local cooling effect of deforestation at higher latitudes. *Nature*, *479*(7373), 384–387. <https://doi.org/10.1038/nature10588>
- Li, Z., Niu, F., Fan, J., Liu, Y., Rosenfeld, D., & Ding, Y. (2011). Long-term impacts of aerosols on the vertical development of clouds and precipitation. *Nature Geoscience*, *4*(12), 888–894. <https://doi.org/10.1038/ngeo1313>
- Liao, H., Seinfeld, J. H., Adams, P. J., & Mickley, L. J. (2004). Global radiative forcing of coupled tropospheric ozone and aerosols in a unified general circulation model. *Journal of Geophysical Research*, *109*, D16207. <https://doi.org/10.1029/2003JD004456>
- Liu, S., Chen, M., & Zhuang, Q. (2014). Aerosol effects on global land surface energy fluxes during 2003–2010. *Geophysical Research Letters*, *41*, 7875–7881. <https://doi.org/10.1002/2014GL061640>
- Marvel, K., Schmidt, G. A., Miller, R. L., & Nazarenko, L. S. (2015). Implications for climate sensitivity from the response to individual forcings. *Nature Climate Change*, *6*, 386–389.
- Mercado, L. M., Bellouin, N., Sitch, S., Boucher, O., Huntingford, C., Wild, M., & Cox, P. M. (2009). Impact of changes in diffuse radiation on the global land carbon sink. *Nature*, *458*(7241), 1014–1017. <https://doi.org/10.1038/nature07949>
- Naudts, K., Chen, Y., McGrath, M. J., Ryder, J., Valade, A., Otto, J., & Luyssaert, S. (2016). Europe's forest management did not mitigate climate warming. *Science*, *351*(6273), 597–600. <https://doi.org/10.1126/science.aad7270>
- Ramanathan, V., Crutzen, P., Kiehl, J., & Rosenfeld, D. (2001). Aerosols, climate, and the hydrological cycle. *Science*, *294*(5549), 2119–2124. <https://doi.org/10.1126/science.1064034>
- Rap, A., Scott, C. E., Reddington, C. L., Mercado, L., Ellis, R. J., Garraway, S., et al. (2018). Enhanced global primary production by biogenic aerosol via diffuse radiation fertilization. *Nature Geoscience*, *11*(9), 640–644. <https://doi.org/10.1038/s41561-018-0208-3>
- Rotstayn, L. D., Collier, M. A., Shindell, D. T., & Boucher, O. (2015). Why does aerosol forcing control historical global-mean surface temperature change in CMIP5 models? *Journal of Climate*, *28*(17), 6608–6625. <https://doi.org/10.1175/JCLI-D-14-00712.1>
- Rubel, F., & Kottke, M. (2010). Observed and projected climate shifts 1901–2100 depicted by world maps of the Köppen-Geiger climate classification. *Meteorologische Zeitschrift*, *19*(2), 135–141. <https://doi.org/10.1127/0941-2948/2010/0430>
- Sarangi, C., Kanawade, V. P., Tripathi, S. N., Thomas, A., & Ganguly, D. (2018). Aerosol-induced intensification of cooling effect of clouds during Indian summer monsoon. *Nature Communications*, *9*(1), 3754. <https://doi.org/10.1038/s41467-018-06015-5>
- Shindell, D. T. (2014). Inhomogeneous forcing and transient climate sensitivity. *Nature Climate Change*, *4*(4), 274–277. <https://doi.org/10.1038/nclimate2136>
- Sicard, M., Bertolin, S., Mallet, M., Dubuisson, P., & Comerón, A. (2014). Estimation of mineral dust long-wave radiative forcing: Sensitivity study to particle properties and application to real cases in the region of Barcelona. *Atmospheric Chemistry and Physics*, *14*(17), 9213–9231. <https://doi.org/10.5194/acp-14-9213-2014>
- Stier, P., Seinfeld, J. H., Kinne, S., & Boucher, O. (2007). Aerosol absorption and radiative forcing. *Atmospheric Chemistry and Physics Discussions*, *7*(19), 5237–5261. <https://doi.org/10.5194/acp-7-5237-2007>
- Stocker, T. F., Qin, D., Plattner, G.-K., Tignor, M. M. B., Allen, S. K., Boschung, J., et al. (2013). *Climate Change 2013: The Physical Science Basis*. Cambridge: Cambridge University Press.
- Streets, D. G., Yan, F., Chin, M., Diehl, T., Mahowald, N., Schultz, M., et al. (2009). Anthropogenic and natural contributions to regional trends in aerosol optical depth, 1980–2006. *Journal of Geophysical Research*, *114*, D00D18. <https://doi.org/10.1029/2008JD011624>
- Stuber, N., Ponater, M., & Sausen, R. (2005). Why radiative forcing might fail as a predictor of climate change. *Climate Dynamics*, *24*(5), 497–510. <https://doi.org/10.1007/s00382-004-0497-7>
- Tang, T., Shindell, D., Faluvegi, G., Myhre, G., Olivie, D., Voulgarakis, A., et al. (2019). Comparison of effective radiative forcing calculations using multiple methods, drivers, and models. *Journal of Geophysical Research: Atmospheres*, *124*, 4382–4394. <https://doi.org/10.1029/2018JD030188>
- Twomey, S. (1991). Aerosols, clouds, and radiation. *Atmospheric Environment A*, *25*(11), 2435–2442. [https://doi.org/10.1016/0960-1686\(91\)90159-5](https://doi.org/10.1016/0960-1686(91)90159-5)
- Wild, M., Folini, D., Henschel, F., Fischer, N., & Müller, B. (2015). Projections of long-term changes in solar radiation based on CMIP5 climate models and their influence on energy yields of photovoltaic systems. *Solar Energy*, *116*, 12–24. <https://doi.org/10.1016/j.solener.2015.03.039>

Erratum

In the originally published version of this article, there were errors in Figure 1. These errors have since been corrected, and the present version may be considered the authoritative version of record.